HHS Public Access

Author manuscript

J Phys Chem Lett. Author manuscript; available in PMC 2021 July 13.

Published in final edited form as:

J Phys Chem Lett. 2019 November 21; 10(22): 7044–7049. doi:10.1021/acs.jpclett.9b02883.

Amine Dynamics in Diamine-Appended Mg_2(dobpdc) Metal–Organic Frameworks

Jun Xu[†,ϕ,*], **Yifei Michelle Liu**[†], **Andrew S. Lipton**[∫], **Jinxing Ye**[†,‡,ϕϕ], **Phillip J. Milner**[‡,§], **Thomas M. McDonald**[‡,ϕϕϕ], **Rebecca L. Siegelman**[‡,§], **Alexander C. Fors**[†,‡,#], **Berend Smit**[†,∫∫], **Jeffrey R. Long**[†,‡,§], **Jeffrey A. Reimer**[†,§]

[†] Department of Chemical and Biomolecular Engineering, University of California, Berkeley, California 94720, United States [‡] Department of Chemistry, and University of California, Berkeley, California 94720, United States [#] Berkeley Energy and Climate Institute, University of California, Berkeley, California 94720, United States [∫] Environmental Molecular Sciences Laboratory, Pacific Northwest National Laboratory, 902 Battelle Boulevard, Richland, Washington 99354, United States [∫∫] Laboratory of Molecular Simulation, Institut des Sciences et Ingénierie Chimiques, Valais Ecole Polytechnique Fédérale de Lausanne (EPFL), Rue de l'Industrie 17, CH-1951 Sion, Switzerland [§] Materials Sciences Division, Lawrence Berkeley National Laboratory, Berkeley, California 94720, United States

Abstract

Variable-temperature ^{15}N solid-state NMR (SSNMR) spectroscopy is used to investigate the dynamics of three diamines within the pores of the metal–organic framework Mg_2(dobpdc), which exhibit both bound and free nitrogen environments when coordinated to the framework open metal sites. From these experiments it is possible to quantify the rates and energetics for exchange between the two nitrogen environments, and the results can then be corroborated by density functional theory calculations and molecular dynamics simulations. The activation energy for the exchange also enables quantification of the metal–amine bond strength, which is correlated with the CO_2 adsorption properties of the diamine-appended frameworks.

[*]Corresponding Author qidongxujun@gmail.com.

[ϕ]**Present Addresses** J.X.: Department of Chemistry and Applied Biosciences, ETH Zürich, Vladimir-Prelog-Weg 1-5, CH-8093 Zürich, Switzerland

[ϕϕ]Y.J.: Engineering Research Center of Pharmaceutical Process Chemistry, Ministry of Education, School of Pharmacy, East China University of Science and Technology, 130 Meilong Road, Shanghai 200237, China

[ϕϕϕ]T.M.M.: Mosaic Materials, Inc., Berkeley, CA 94720, United States

ASSOCIATED CONTENT

Supporting Information. Additional information including elucidated CO_2 adsorption mechanism, sample preparation, characterizations, theoretical calculations, rate constant calculations and additional discussions. DFT-optimized structures. Movie of diamine exchange. The following files are available free of charge via the Internet at http://pubs.acs.org. Electronic Supporting Information (PDF)

DFT-optimized Structure (CIF)

Movie of diamine exchange (MPG)

The authors declare the following competing financial interest(s): T.M.M. and J.R.L. have a financial interest in Mosaic Materials, Inc., a start-up company working to commercialize metal–organic frameworks for gas separations. UC Berkeley has applied for a patent on some of the materials discussed herein, on which T.M.M. and J.R.L. are included as inventors.

TOC GRAPHIC

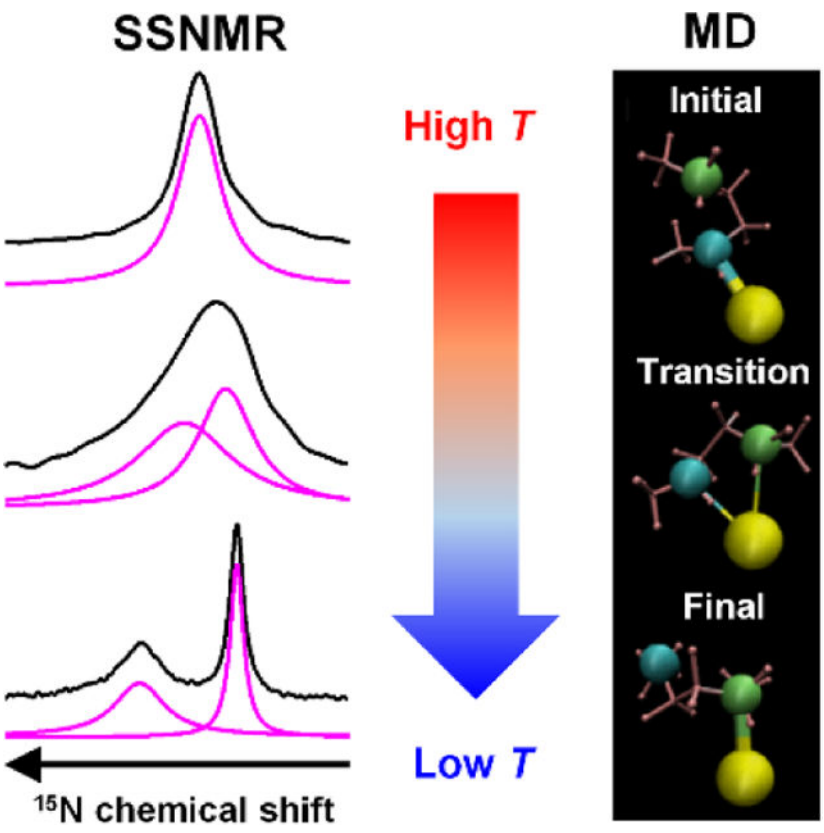

Rising anthropogenic CO_2 emissions remain the leading source of global climate change,[1] and the capture and sequestration of CO_2 from power plant flue gas emissions has been highlighted as a potentially promising emission mitigation strategy in recent years.[2–4] Numerous approaches have been developed for the removal of CO_2 from flue gas through the use of aqueous amine solutions,[4] zeolites,[5] metal−organic frameworks (MOFs),[6] and covalent organic frameworks.[7] Metal−organic frameworks with coordinatively-unsaturated metal centers such as the M_2(dobdc) family (dobdc^{4-} = 2,5-dioxido-1,4-benzenedicarboxylate; M = Mg, Mn, Fe, Co, Ni, Cu, Zn) have attracted considerable attention owing to the strong interaction that occurs between the metal centers and CO_2 upon adsorption, which leads to a high affinity for CO_2 adsorption and selectivity over N_2. One drawback of these materials, however, is that their performance often diminishes under humid conditions.[8–10] Recently, it was demonstrated that after grafting diamines onto the open metal sites of Mg_2(dobpdc) (dobpdc^{4-} = 4,4′-dioxidobiphenyl-3,3′-dicarboxylate), an expanded form of Mg_2(dobdc), the resulting material exhibits substantially improved CO_2 adsorption properties arising from step-shaped adsorption isotherms (or isobars) that allow for high working capacities in temperature- or pressure-swing adsorption processes and robust performance under humid conditions.[10–15] Notably, the step pressure (or temperature) can be tuned through variation of the appended diamine,[11–15] and it is thus of fundamental importance to investigate in detail the influence of diamine structure on the CO_2 adsorption properties of diamine-appended Mg_2(dobpdc) materials.

The structures of diamine-appended variants of Mg_2(dobpdc), such as the *N,N′*-dimethylethylenediamine (m-2-m)-appended framework (Figure 1), have one nitrogen coordinated to Mg^{2+}, while the other amine group extends into the open MOF pore. Above a threshold temperature and pressure, CO_2 inserts into the Mg−N bond, resulting in the formation of a carbamate group bound to magnesium center and an ammonium group formed at the other end of the diamine (Figure S1, Supporting Information). The interaction between the negative carbamate and a neighboring positive ammonium facilitates the synergistic formation of ammonium–carbamate chains along the framework channels, leading to the observed cooperative adsorption behavior.[11,16] As a consequence, the metal–amine bond strength plays an important role in determining the pressure or temperature at which CO_2 insertion occurs. This effect has been examined recently via single-crystal X-ray diffraction characterization of the isostructural diamine-appended Zn_2(dobpdc) frameworks,[13] which readily form single crystals. Even still, these single-crystal structures exhibit a large degree of diamine disorder within the framework channels at 100 K, and so we sought to develop additional approaches for assessing the structures, particularly for the diamine-appended Mg_2(dobpdc) variants. We were specifically interested in exploring the dynamic behavior of the diamines within the MOF pores, as a potential means of guiding the design of new diamine-appended structures for CO_2 capture.

Solid-state NMR (SSNMR) spectroscopy is complementary to X-ray diffraction as a characterization technique and is extremely sensitive to the local environment around the observed nucleus. The subtle difference between the bound and free nitrogen environments of diamines should in particular be detectable by ^{15}N SSNMR spectroscopy.[17,18] Although the ^{15}N SSNMR spectrum of m-2-m–Mg_2(dobpdc) was previously found to exhibit a single ^{15}N peak at room temperature,[11] a recent ^{25}Mg SSNMR study indicated that the two nitrogen environments undergo rapid exchange, yielding an averaged environment on the NMR time scale.[19] Herein, we analyze variable-temperature (VT) ^{15}N SSNMR data to probe the nitrogen environments and dynamics of three diamines appended to Mg_2(dobpdc), namely ethylenediamine (en), *N,N′*-dimethylethylenediamine (m-2-m), and *N,N′*-diethylethylenediamine (e-2-e). In each case, the NMR data enable elucidation of the diamine dynamics within the framework, yielding activation energies for diamine exchange that provide a measure of the metal−amine bond strength. When combined with density functional theory (DFT) calculations and molecular dynamics (MD) simulations, these results provide insights into correlations between diamine structure and the CO_2 adsorption properties of these materials.

The variable-temperature ^{15}N SSNMR spectra of en–Mg_2(dobpdc) are shown in Figure 2. At 298 K, a symmetric ^{15}N peak arises at 12.7 ppm. This peak broadens considerably upon cooling to 233 K and then becomes asymmetric at 223 K, eventually separating into two peaks upon further cooling. The separation between these two new peaks continues to increase with decreasing temperature, while their characteristic line widths (full width at half maximum) decrease. At the lowest measurement temperature of 183 K, the two peaks are observed at 11.4 and 14.8 ppm (relative to neat NH_3), respectively. This overall trend as a function of temperature is consistent with the rapid exchange between two nitrogen environments.[20–24] We assigned the peaks at 14.8 and 11.4 ppm to the metal-bound and free amine nitrogen environments, respectively, considering that nitrogen will be deshielded by

the Mg^{2+} cation and experience a larger ^{15}N chemical shift value. This assignment was verified by DFT calculations (Figure S6).

Deconvolution of the SSNMR spectra enables determination of the frequency separation between the two ^{15}N peaks and their line widths, and from this information it is possible to calculate a chemical exchange rate constant. For example, in the range where the peak positions exhibit a strong temperature dependence (223–208 K), the exchange rate constant k_E was calculated using the equation $k_E = \pi\sqrt{(\Delta\upsilon_o^2 - \Delta\upsilon_e^2)}/\sqrt{2}$, where $\Delta\upsilon_o$ is the frequency separation between two peaks (in Hz) without exchange and $\Delta\ \upsilon_e$ is the separation with exchange.[20–24] The exchange rate constant was found to be $3.16 \times 10^2\ s^{-1}$ at 213 K, and the calculation details for all k_E values are shown in Supporting Information Section S5 (Table S3).

The same variable-temperature analysis was used to assess the dynamics of m-2-m and e-2-e appended to Mg_2(dobpdc). At 293 K, the spectrum of m-2-m consists of an asymmetric peak at 13.3 ppm and a weak shoulder at ~20 ppm (Figure 3a). Upon cooling, the asymmetric peak narrows and shifts to the more shielded region of the spectrum (lower ppm values). This peak can be deconvoluted into two components at all temperatures, and at 193 K the deconvoluted peaks occur at 16.7 and 15.7 ppm for the bound and free nitrogen environments, respectively. The chemical shift value of the shoulder is close to that of the single 15N resonance observed for free *N,N′*-dimethylethylenediamine in toluene, and was assigned to the unbound amine trapped in the MOF pores. Characterization of a second m-2-m–Mg_2(dobpdc) sample verified the above peak assignments and the changes in peak position as a function of temperature (Figures S12 and S14, Supporting Information).

The variable-temperature spectra of e-2-e–Mg_2(dobpdc) are likewise shown in Figure 3b. At 313 K, a single ^{15}N peak is apparent at 34.6 ppm and grows asymmetric at 283 K, eventually splitting into two peaks upon further cooling. The peak separation increased with decreasing temperature, and at the lowest measured temperature (223 K), the two resulting peaks were at 36.0 and 28.7 ppm for the bound and free nitrogen environments, respectively. Similar to m-2-m–Mg_2(dobpdc), a weak shoulder was present at ~40 ppm in all spectra and can be assigned to unbound *N,N′*-diethylethylenediamine in the pores (Figure S14). For both frameworks, these diamines were not observed to participate in the exchange (see Figure S15 and the following discussion). The separation of the coordinated diamine nitrogen peaks increased significantly even at the lowest measured temperature for both materials, and thus it was not possible to determine $\Delta\ \upsilon_o$ and the precise exchange rate constants for m-2-m and e-2-e appended frameworks. It was possible to calculate a potential range of k_E values, however, and this data (Table S3) along with additional discussions can be found in Supporting Information Section S5.

Using the Arrhenius equation and the rate constants obtained from SSNMR data, it was possible to determine the activation energy for free and bound nitrogen exchange in each material (Table 1). A much larger activation energy was found for en ($37 \pm 2\ kJ{\cdot}mol^{-1}$) than for m-2-m and e-2-e (ranging from 0.67 ± 0.06 to $6.4 \pm 1.5\ kJ{\cdot}mol^{-1}$ and from 0.83 ± 0.05 to $10.9 \pm 0.9\ kJ{\cdot}mol^{-1}$, respectively), indicating that the substitution of an amine hydrogen with

an alkyl group (i.e., changing the bound amine from primary to secondary) significantly weakens the metal–amine bond. The result is consistent with single-crystal X-ray diffraction data for the Zn analogues,[13] which confirms that primary/secondary and primary/tertiary diamines preferentially coordinate to the Zn^{2+} centers through the primary amine.

Molecular dynamics (MD) simulations have been used extensively to study flexibility and guest dynamics in metal−organic frameworks,[19,25–29] and we used this approach to further examine the dynamics and compute exchange rates for the diamines appended to Mg_2(dobpdc). In order to capture the bond breaking and formation in the exchange event, we employed the ReaxFF, a reactive force field based on bond order.[25,30] The simulation results confirm exchange between the bound and free nitrogen atoms (see Figure 4, Figure S7, and the movie in the Supporting Information) and enable identification of a possible exchange mechanism, with a transition state consisting of both nitrogen atoms of the diamine molecule weakly bound to the same Mg^{2+} center. The calculated kinetic activation energies (E_A) in Table 1 have similar magnitudes and display the same trend as the experimental values: the activation energy for m-2-m is smaller than that of e-2-e, and both values are smaller than the experimental value for en.

As previously elucidated, the CO_2 adsorption mechanism in these diamine-appended materials involves the insertion of CO_2 into the metal−amine bonds and the synergistic formation of ammonium−carbamate chains (Figure S1).[11,16] Because the metal−amine bonds are broken upon CO_2 adsorption, stronger bonds and therefore higher activation energies for nitrogen exchange are expected to correlate with higher adsorption step pressures (or lower step temperatures). The opposite trend was observed experimentally, with step pressure decreasing in the order m-2-m > e-2-e > en, despite the larger activation barrier toward exchange for en compared to m-2-m and e-2-e.[11–14] Therefore, our NMR data and MD simulations confirm that the metal−amine bond strength is not the only important factor in determining the adsorption step pressure. Other factors can also influence the thermodynamics of adsorption,[13] such as the carbamate enthalpy of formation and the loss of rotational and vibrational degrees of freedom upon ammonium−carbamate chain formation (i.e., large negative entropy change).

In conclusion, we used variable-temperature ^{15}N SSNMR spectroscopy to characterize the coexistence of bound and free nitrogen environments in three diamine-appended variants of the Mg_2(dobpdc) metal−organic framework, and further identified a likely transition state involved in nitrogen exchange from MD simulations. The magnitude of the activation energies extracted from both SSNMR experiments and MD simulations afforded a measure of metal−amine bond strength, indicating that m-2-m– and e-2-e–Mg_2(dobpdc) materials have similar bond strengths that are both weaker than the metal−amine bond strength for en–Mg_2(dobpdc). The trends in the experimental data were verified by DFT calculations and MD simulations, and all together the data confirm that the metal−amine bond strength is not the only important determiner of CO_2 adsorption step pressure. The approach described herein can be importantly extended to other diamine-appended metal−organic frameworks to understand diamine dynamics and CO_2 adsorption toward the design of improved carbon capture materials.

Supplementary Material

Refer to Web version on PubMed Central for supplementary material.

ACKNOWLEDGMENT

This work was supported through the Center for Gas Separations Relevant to Clean Energy Technologies, an Energy Frontier Research Center funded by the U.S. Department of Energy, Office of Science, Basic Energy Sciences, under Award DE-SC0001015. The 20.0 T variable-temperature ^{15}N SSNMR experiments were performed at the Environmental Molecular Sciences Laboratory, a DOE Office of Science User Facility sponsored by the Office of Biological and Environmental Research. DFT calculations were performed on the Dino cluster in the Molecular Graphics and Computation Facility at UC Berkeley, which is funded by the U.S. National Institutes of Health under Award S10OD023532. The MD simulations were carried out at the National Energy Research Scientific Computing Center, a User Facility supported by the Office of Science of the U.S. Department of Energy under Contract DE-AC02–05CH11231. We thank the NSF Graduate Research Fellowship program for support of Y.M.L. We thank the National Institute of General Medical Sciences of the National Institutes of Health for a postdoctoral fellowship for P.J.M. (F32GM120799). We thank Prof. Gina L. Hoatson and Dr. Rony Kalfarisi for use of a 750 MHz spectrometer in College of William and Mary, United States, during initial attempts to collect ^{15}N variable-temperature SSNMR data. We thank Dr. Jeffrey Martell for experimental assistance and fruitful discussions, and Dr. Katie Meihaus for editorial assistance.

REFERENCES

(1). IPCC. Contributions of Working Group I to the Fifth Assessment Report of the Intergovernmental Panel on Climate Change. In Climate Change 2013: The Physical Science Basis; Stocker TF, Qin D, Plattner G-K, Tignor MMB, Allen SK, Boschung J, Nauels A, Xia Y, Bex V, Midgley PM, Eds.; Cambridge University Press: Cambridge, United Kingdom and New York, 2013.

(2). IPCC IPCC Special Report on Carbon Dioxide Capture and Storage, Cambridge University Press: Cambridge, United Kingdom and New York, 2005.

(3). Bhown AS; Freeman BC Analysis and Status of Post-Combustion Carbon Dioxide Capture Technologies. Environ. Sci. Technol. 2011, 45, 8624–8632. [PubMed: 21905745]

(4). Schimming V; Hoelger C-G; Buntkowsky G; Sack I; Fuhrhop J-H; Rocchetti S; Limbach H-H Evidence by 15N CPMAS and 15N−13C REDOR NMR for Fixation of Atmospheric CO2 by Amino Groups of Biopolymers in the Solid State. J. Am. Chem. Soc. 1999, 121, 4892–4893.

(5). Choi S; Drese JH; Jones CW Adsorbent Materials for Carbon Dioxide Capture from Large Anthropogenic Point Sources. ChemSusChem 2009, 2, 796–854. [PubMed: 19731282]

(6). Sumida K; Rogow DL; Mason JA; McDonald TM; Bloch ED; Herm ZR; Bae T-H; Long JR Carbon Dioxide Capture in Metal–Organic Frameworks. Chem. Rev. 2012, 112, 724–781. [PubMed: 22204561]

(7). Zeng Y; Zou R; Zhao Y. Covalent Organic Frameworks for CO2 Capture. Adv. Mater. 2016, 28, 2855–2873. [PubMed: 26924720]

(8). Kizzie AC; Wong-Foy AG; Matzger AJ Effect of Humidity on the Performance of Microporous Coordination Polymers as Adsorbents for CO2 Capture. Langmuir 2011, 27, 6368–6373. [PubMed: 21488612]

(9). Yu J; Balbuena PB Water Effects on Postcombustion CO2 Capture in Mg-MOF-74. J. Phys. Chem. C 2013, 117, 3383–3388.

(10). Mason JA; McDonald TM; Bae T-H; Bachman JE; Sumida K; Dutton JJ; Kaye SS; Long JR Application of a High-Throughput Analyzer in Evaluating Solid Adsorbents for Post-Combustion Carbon Capture via Multicomponent Adsorption of CO2, N2, and H2O. J. Am. Chem. Soc. 2015, 137, 4787–4803. [PubMed: 25844924]

(11). McDonald TM; Mason JA; Kong X; Bloch ED; Gygi D; Dani A; Crocella V; Giordanino F; Odoh SO; Drisdell WS et al. Cooperative Insertion of CO2 in Diamine-Appended Metal-Organic Frameworks. Nature 2015, 519, 303–308. [PubMed: 25762144]

(12). McDonald TM; Lee WR; Mason JA; Wiers BM; Hong CS; Long JR Capture of Carbon Dioxide from Air and Flue Gas in the Alkylamine-Appended Metal–Organic Framework mmen-Mg2(dobpdc). J. Am. Chem. Soc. 2012, 134, 7056–7065. [PubMed: 22475173]

(13). Siegelman RL; McDonald TM; Gonzalez MI; Martell JD; Milner PJ; Mason JA; Berger AH; Bhown AS; Long JR Controlling Cooperative CO2 Adsorption in Diamine-Appended Mg2(dobpdc) Metal–Organic Frameworks. J. Am. Chem. Soc. 2017, 139, 10526−10538.

(14). Lee WR; Hwang SY; Ryu DW; Lim KS; Han SS; Moon D; Choi J; Hong CS Diamine-Functionalized Metal-Organic Framework: Exceptionally High CO2 Capacities from Ambient Air and Flue Gas, Ultrafast CO2 Uptake Rate, and Adsorption Mechanism. Energ. Environ. Sci. 2014, 7, 744–751.

(15). Milner PJ; Siegelman RL; Forse AC; Gonzalez MI; Runčevski T; Martell JD; Reimer JA; Long JR A Diaminopropane-Appended Metal–Organic Framework Enabling Efficient CO2 Capture from Coal Flue Gas via a Mixed Adsorption Mechanism. J. Am. Chem. Soc. 2017, 139, 13541−13553.

(16). Vlaisavljevich B; Odoh SO; Schnell S; Dzubak AL; Lee K; Planas N; Neaton J; Gagliardi L; Smit B. CO2 Induced Phase Transitions in Diamine-Appended Metal Organic Frameworks. Chem. Sci. 2015, 6, 5177–5185. [PubMed: 28717499]

(17). Witanowski M; Stefaniak L; Webb GA Nitrogen NMR Spectroscopy. Annu. Rep. NMR Spectrosc. 1993, 25, 1–480.

(18). Mason J. Nitrogen NMR. In Encycl. NMR; Harris RK, Wasylishen RE, Eds.; John Wiley & Sons, Ltd, 2012; Vol. 5.

(19). Xu J; Blaakmeer ESM; Lipton AS; McDonald TM; Liu YM; Smit B; Long JR; Kentgens APM; Reimer JA Uncovering the Local Magnesium Environment in the Metal–Organic Framework Mg2(dobpdc) Using 25Mg NMR Spectroscopy. J. Phys. Chem. C 2017, 121, 19938−19945.

(20). McConnell HM Reaction Rates by Nuclear Magnetic Resonance. J. Chem. Phys. 1958, 28, 430–431.

(21). Abragam A. The Principles of Nuclear Magnetism, Clarendon Press: Oxford, 1961.

(22). Bain AD Chemical Exchange in NMR. Prog. Nucl. Magn. Reson. Spectrosc. 2003, 43, 63–103.

(23). Alexander S. Exchange of Interacting Nuclear Spins in Nuclear Magnetic Resonance. II. Chemical Exchange. J. Chem. Phys. 1962, 37, 974–980.

(24). Limbach H-H; Wehrle B; Schlabach M; Kendrick R; Yannoni CS CPMAS Polarization Transfer Methods for Superposed Chemical Exchange and Spin Diffusion in Organic Solids. J. Magn. Reson. 1988, 77, 84–100.

(25). Huang L; Joshi KL; Duin A. C. T.v.; Bandosz TJ; Gubbins KE ReaxFF Molecular Dynamics Simulation of Thermal Stability of a Cu3(BTC)2 Metal-Organic Framework. Phys. Chem. Chem. Phys. 2012, 14, 11327−11332.

(26). Getman RB; Bae Y-S; Wilmer CE; Snurr RQ Review and Analysis of Molecular Simulations of Methane, Hydrogen, and Acetylene Storage in Metal–Organic Frameworks. Chem. Rev. 2012, 112, 703–723. [PubMed: 22188435]

(27). Lin L-C; Kim J; Kong X; Scott E; McDonald TM; Long JR; Reimer JA; Smit B. Understanding CO2 Dynamics in Metal–Organic Frameworks with Open Metal Sites. Angew. Chem. Int. Ed. 2013, 52, 4410–4413.

(28). Boyd PG; Moosavi SM; Witman M; Smit B. Force-Field Prediction of Materials Properties in Metal-Organic Frameworks. J. Phys. Chem. Lett. 2017, 8, 357–363. [PubMed: 28008758]

(29). Jawahery S; Simon CM; Braun E; Witman M; Tiana D; Vlaisavljevich B; Smit B. Adsorbate-Induced Lattice Deformation in IRMOF-74 Series. Nat. Commun. 2017, 8, 13945.

(30). van Duin ACT; Dasgupta S; Lorant F; Goddard WA ReaxFF: A Reactive Force Field for Hydrocarbons. J. Phys. Chem. A 2001, 105, 9396–9409.

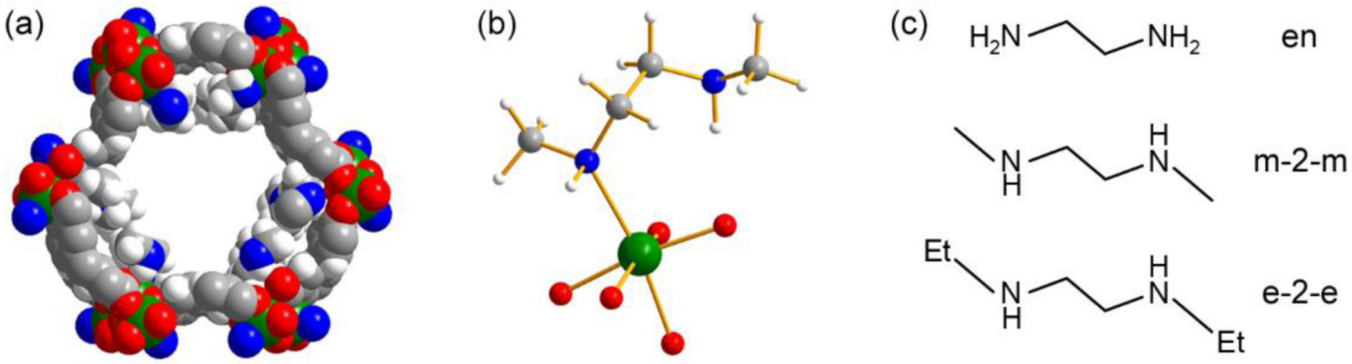

Figure 1.

(a) Space-filling model of Mg_2(dobpdc) appended with *N,N′*-dimethylethylenediamine, m-2-m–Mg_2(dobpdc), and (b) Ball-and-stick model of an m-2-m-appended Mg^{2+} site within the framework, with bound and free nitrogen environments. The models are taken from the DFT-optimized structures reported in this work. Green, red, blue, grey, and white spheres represent Mg, O, N, C, and H atoms, respectively; all other H atoms are omitted for clarity. (c) The structures of three diamines studied in this work.

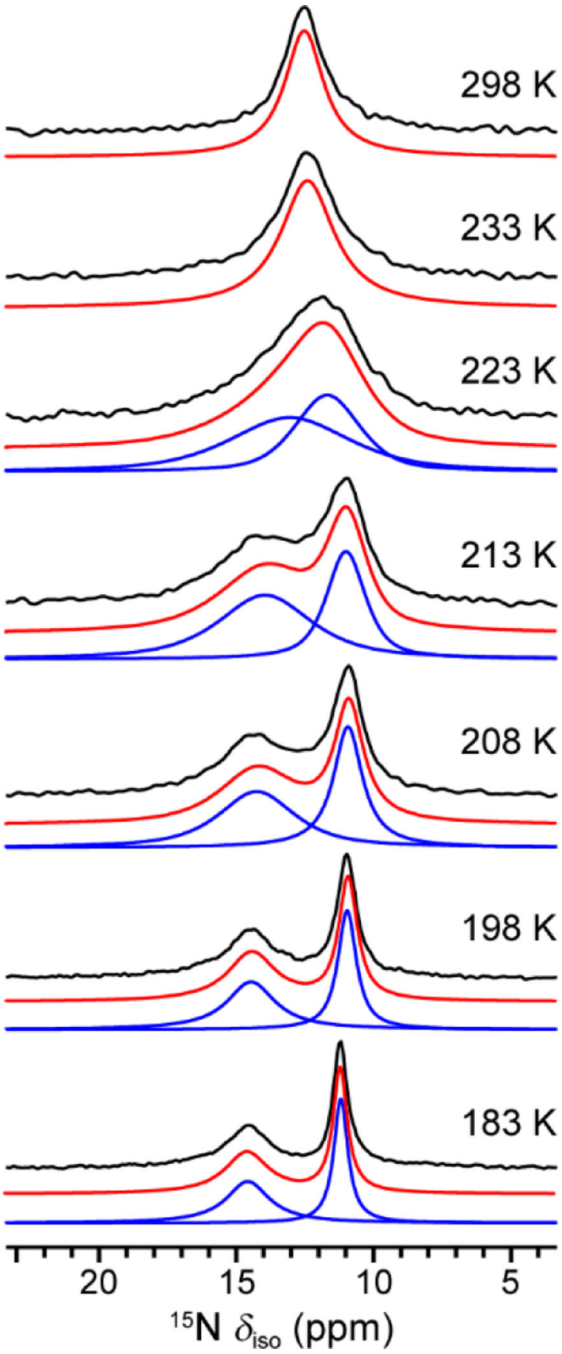

Figure 2.

^{15}N direct-polarization SSNMR spectra of en–Mg_2(dobpdc) at 20.0 T as a function of temperature. Black, blue, and red profiles are experimental, deconvoluted, and the summation of deconvoluted spectra, respectively. The signal intensities are normalized for clarity.

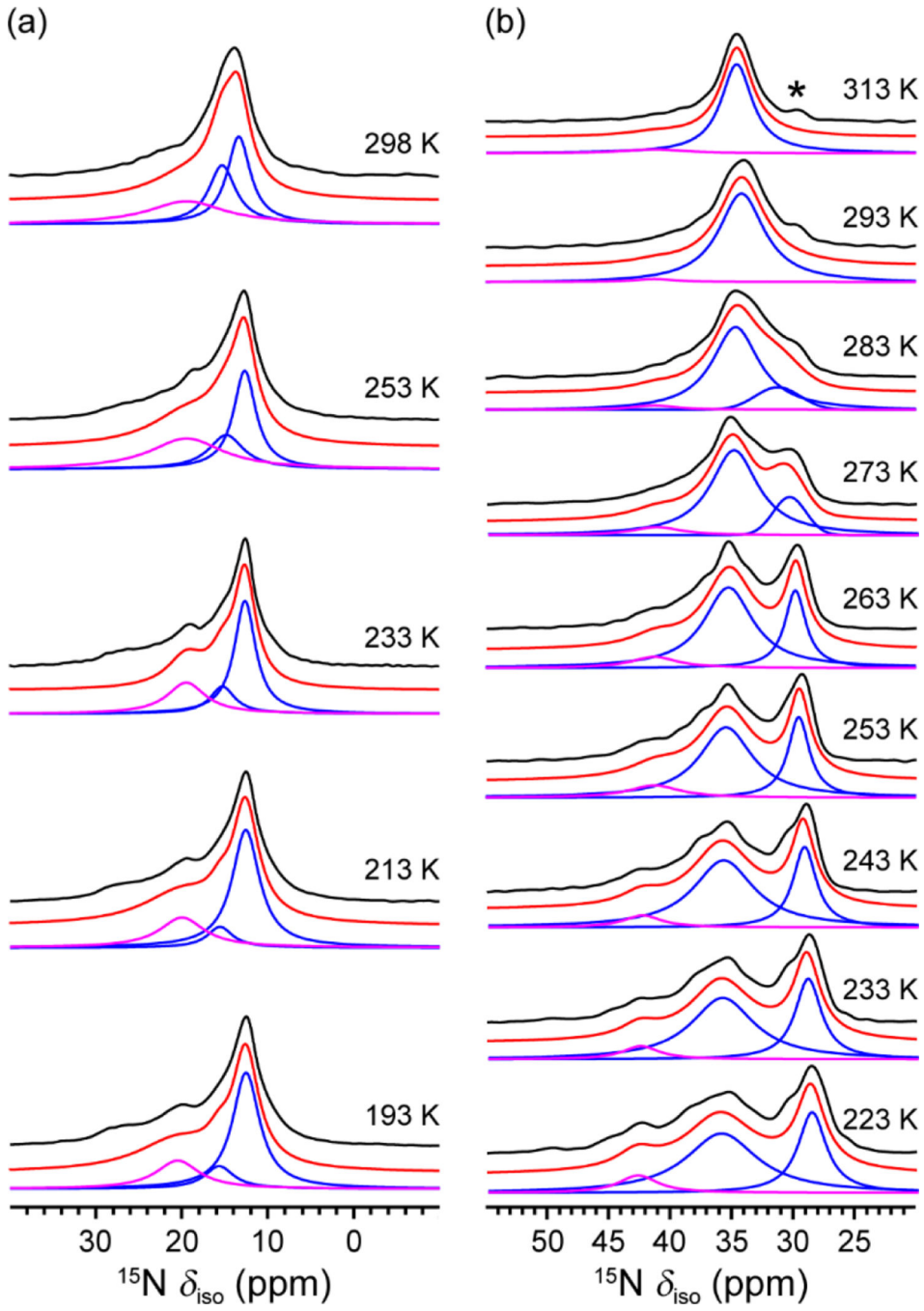

Figure 3.

(a) ^{1}H–^{15}N cross-polarization (CP) SSNMR spectra of m-2-m–Mg_2(dobpdc) as a function of temperature. (b) ^{1}H–^{15}N CP SSNMR spectra of e-2-e–Mg_2(dobpdc) as a function of temperature. Black profiles are experimental spectra. Blue and pink profiles are deconvoluted spectra. Red profiles are the summation of deconvoluted spectra. Pink profiles represent the ^{15}N signals that were assigned to unbound diamines trapped in the MOF pores (Figure S14). All signal intensities are normalized for clarity. The asterisk in the 313 K data indicates signal arising from the transmitter artifact. ^{1}H–^{15}N CP experiments were

performed at 20.0 T with a contact time of 5 ms for m-2-m–Mg_2(dobpdc) and at 16.4 T with a contact time of 0.5 ms for e-2-e–Mg_2(dobpdc).

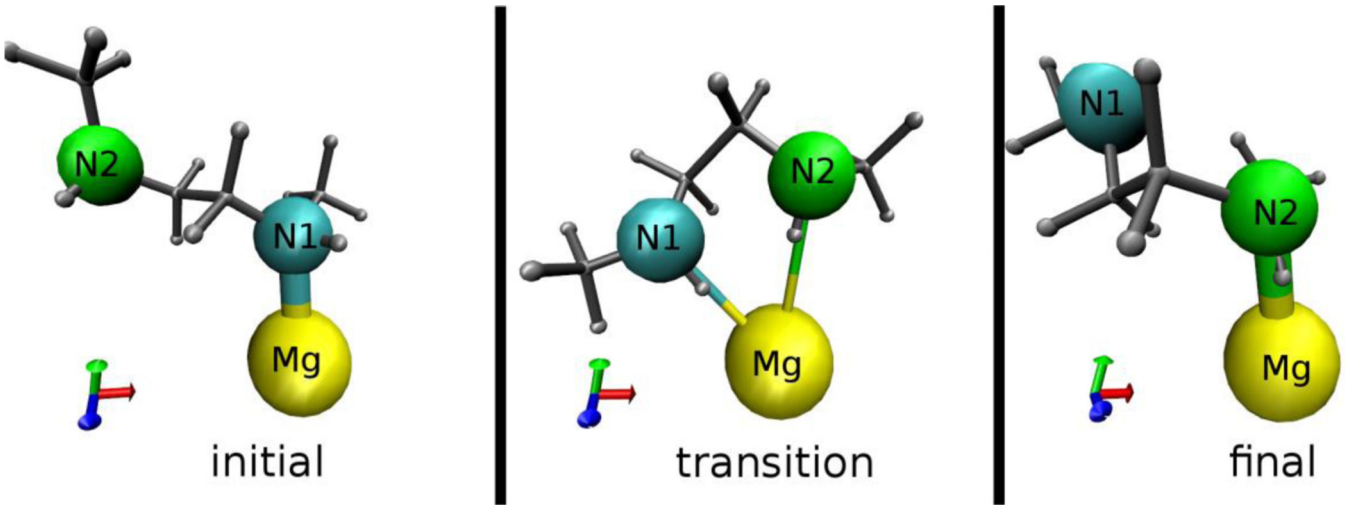

Figure 4.

Still frames from the MD trajectory illustrating representative initial, transition, and final states for the amine nitrogen atoms in an m-2-m exchange event. In the transition state, the nitrogen that is initially unbound (N2) coordinates to the Mg^{2+} center, and in the final state the initially bound nitrogen (N1) becomes free.

Table 1.

Activation energies of three diamines appended to Mg_2(dobpdc).

Diamine	E_A **(kJ·mol^{-1})**	
	Experimental	Calculated
en	37 ± 2	
m-2-m	0.67 ± 0.06–6.4 ± 1.5	7.93 ± 1.41
e-2-e	0.83 ± 0.05–10.9 ± 0.9	10.5 ± 1.3